

# Flight Tour Planning with Recharging Optimization for Battery-operated Autonomous Drones

Chien-Ming Tseng, Chi-Kin Chau, Khaled Elbassioni and Majid Khonji

**Abstract**—Autonomous drones (also known as unmanned aerial vehicles) have several advantages over ground vehicles, including agility, swiftness, and energy-efficiency, and hence are convenient for light-weight delivery and substitutions for manned missions in remote operations. It is expected that autonomous drones will be deployed in diverse applications in near future. Typical drones are electric vehicles, powered by on-board batteries. This paper presents several contributions for automated battery-operated drone management systems: (1) We conduct an empirical study to model the battery performance of drones, considering various flight scenarios. (2) We study a joint problem of flight tour planning with recharging optimization for drones with an objective to complete a tour mission for a set of sites of interest. This problem captures diverse applications of delivery and remote operations by drones. (3) We implemented our optimization algorithms in an intelligent drone management system.

**Index Terms**—Drones, Electric Vehicles, Flight Tour Planning, Recharging Optimization, Intelligent Drone Management System

## I. INTRODUCTION

Aerial vehicles are becoming a vital transportation means. Often referred as drones in popular terminology, or unmanned aerial vehicles in technical terminology, they have several advantages over ground vehicles as follows. (1) *Agility*: There is little restriction in the sky, unlike on the ground with obstacles. Drones can travel across space in straight paths. They are usually small in size, with nimble navigating ability. (2) *Swiftness*: Aerial transportation is usually not hampered by traffic congestions. The time to arrival is mostly reflected by the travelled distance. Drones can also be rapidly launched by catapults, and drop off payloads by parachutes with short response time. (3) *Energy-efficiency*: Drones are typically light-weight, which consume less energy. They are particularly energy-efficient for transporting light-weight items in short trips, whereas ground vehicles are useful for carrying heavy objects in long distance. (4) *Safeness*: There is no on-board human operator or driver. Drones can keep a safe distance from human users. Unmanned transportation missions are specially desirable in hazardous environments. (5) *Low-cost*: Drone platforms and systems have evolved to be a mature technology. There are a variety of open-source projects for both drone hardware and software systems. The specifications of drones can vary flexibly according to different form factors and costs.

These advantages of drones enable diverse applications for light-weight goods transportation and substitutions for manned transportation missions. Some examples are provided

as follows. (1) *Remote Surveillance*: Aerial transportation can access far-away remote regions, geographically dispersed and offshore locations. Particularly, oil and gas companies and utility providers, which rely on extensive surveillance, measurements, mapping and surveying, maintenance operations for dispersed facilities, will be major users of drones. (2) *Search and Rescue*: Drones can be deployed in ad hoc manner. In emergency with damaged or unreliable infrastructure, drones can overcome the difficulty of accessing in isolated regions, enabling fast transportation with great convenience and flexibility. (3) *Hazardous Missions*: Drones are excellent solutions for unmanned missions in risky or hazardous areas, in particular, for taking measurements in high-altitude, or bio/chemical harmful environments. Human supervisors can remotely control the drones to carry out dangerous operations. (4) *Light-weight Items Delivery*: Parcels, medical items, and mail require speedy delivery. Drones are effective in solving the last-leg problem of the distribution chain from depots to homes of end-users. A recent study by Amazon [1] reports that 44% of the US population are within 20 miles from its depot facility. Hence, it is practical to employ drone delivery.

In the near future, fully autonomous drones are expected for extensive deployment, giving rise to a new class of intelligent transportation system. Despite increasingly popular applications of drones in diverse sectors, the management of drones is plagued with several challenges:

- *Limited Battery Lifetime*: Typical drones are electric vehicles, powered by on-board batteries. Hence, the performance of drones is critically constrained by limited battery lifetime. Many drones are only suitable for short-range trips, which considerably limit their applicability. To optimize the battery performance of drones, there requires an intelligent management system to track state-of-charge, and optimize their operations accordingly.
- *Control Difficulty*: Piloting a drone is difficult for human. Manual controls not only incur inefficiency and inconvenience, but also are vulnerable to human errors. Often, intensive trainings for drone piloting are required in advance, which are usually expensive and laborious. Improper human controls will cause drone crashes and damages. There are routine missions that are suitable for drones with minimal manual controls.
- *Dynamic Operating Environments*: Drones are expected to travel in certain high altitude, and hence are significantly susceptible by wind and weather conditions. These conditions are highly dynamic, and should be accounted for in a real-time manner. Also, drones are light-weight,

C.-M. Tseng, C.-K. Chau, K. Elbassioni and M. Khonji are with the Department of EECS, Masdar Institute of Science and Technology, UAE (e-mail: {ctseng, ckchau, kelbassioni, mkhonji}@masdar.ac.ae).

and the impact by wind is even more substantial. Drone management system should take explicit consideration of the dynamic uncertain operating environments.

These challenges present a unique class of vehicle management problem for battery-operated autonomous drones.

#### A. Our Contributions

To support diverse applications of drones in practice, this paper presents several contributions for automated battery-operated drone management systems:

- 1) We conduct an empirical study to model the energy consumption of drones, considering various flight scenarios. Accurate model of battery performance in different scenarios allows further flight tour planning with recharging optimization for drone missions.
- 2) We study a joint problem of flight tour planning with recharging optimization for drones with an objective to complete a tour mission for a set of sites of interest in the shortest time. We consider a variable number of charging stations for recharging drones intermediately. This problem captures diverse applications of delivery and remote operations by drones. The solution of this problem will be useful for an intelligent drone management system.
- 3) We implemented our algorithms in an intelligent drone management system, which supports real-time flight path tracking and re-computation in dynamic environments.

We remark that our study can also provide ramifications to general electric vehicle management. Our study of flight tour planning with recharging optimization applies to various electric vehicle fleet. In the future, battery-operated flying vehicles, which resemble today's drones, will be able to carry both passengers and goods in the sky [2]. Our study can be extended to future flying electric vehicles.

## II. RELATED WORK

There are diverse applications for drones, including delivery (e.g., for light-weight parcels, medical items, mail) and remote operations (e.g., wildlife surveillance, environmental surveying, search and rescue operations). Drones have been extensively studied for their flight and landing control mechanisms. For example, see the books [3], [4] for a good overview of the recent results. The literature usually concerns the control system of individual drones. However, these studies typically focus on a single short-distance flight path and transient control regarding the flight movements. Long-distance flight tour planning involving multiple paths with recharging optimization has been considered to a lesser extent, to the best of our knowledge. Moreover there is a lack of related work on optimizing the flight plans of battery-operated drones.

The logistic optimization of electric vehicles have been studied mainly for ground vehicles. Nonetheless, drones exhibit different characteristics that create some unique challenges. For example, the impact of wind is more substantial for drone flight. In [5], graph signal sampling and recovery techniques

are used to plan routes for autonomous aerial vehicles, and a method is proposed to plan an energy-efficient flight trajectory by considering the influences of wind. Further, there appears limited empirical studies of battery performance of drones, although empirical studies of electric ground vehicles have been explored in the literature.

Modelling vehicle energy consumption has been the subject of a number of research papers. One method is the model-based approach, based on vehicle dynamics to model the consumption behavior of electric vehicles [6]. Energy consumption estimation can use a blackbox approach. For example, a statistical approach using regression model to estimate energy consumption of vehicles is given in [7].

This work belongs to the scope of path planning problem of electric vehicles. There are recent results for path planning of electric vehicles considering recharging operations [8], [9]. We adopt the solution proposed in [10] for the so-called tour gas station problem, for which efficient algorithms are designed for obtaining a near-optimal solution under certain assumptions. A variant of the classical algorithm [11] for the travelling salesman problem (TSP) was proposed in [10] for the tour gas station problem. In this work, we extend those methods to solve the problem for drone management and consider extensions to more realistic settings, such as time minimization.

For fully autonomous drone management, drones should also be able to recharge themselves without manual intervention. To enable autonomous recharging of drones, autonomous inductive charging systems has been proposed in [12], which can be integrated with the management system of this paper.

## III. EMPIRICAL STUDY OF ENERGY CONSUMPTION

In order to accurately optimize the energy consumption and flight paths of a drone, we conduct an empirical study to determine its battery performance, considering various flight scenarios. In particular, we evaluate the energy consumption using a commercial drone model, 3DR Solo (see Fig. 1 and its specifications in Table I). 3DR Solo drone supports Python developer kit, which allows us to extract data and program the flight path. After gathering sufficient measurement data, we apply a regression model to capture the energy consumption of the test drone.



Fig. 1: 3DR Solo as test drone.

#### A. Empirical Study

A typical drone is equipped with a number of sensors for two purposes: (1) self-stabilizing the drone in the air,

	Specifications
Weight	2 kg
Dimensions	25cm × 46cm
Battery	5200 mAh 14.8V
Motors	880 kV (×4)
Max Speed	40 km/h
Max Altitude	122 ft (FAA Regulation)
Charging Time	90 mins
Software	Python Developer Kit

TABLE I: Specifications of 3DR Solo drone.

and (2) remotely tracking the drone status (e.g., the battery state-of-charge (SoC)). The stability of drone is controlled by three essential sensors (i.e., gyroscopes, accelerometers and barometers), with which it can maneuver itself in the air. The SoC is measured by the voltage and current sensors. A major part of energy consumption of a drone is required for powering the motors to lift the drone itself in the air. Additional energy consumption is required for the movements of the drone. The movements can be decomposed into vertical and horizontal directions. The barometer and GPS sensors can measure the 3-dimensional movements of the drone. The speed and position of the drone can be tracked by GPS and IMU modules, which also enable automatic navigation. The altitude of the drone can be tracked by barometer and GPS modules.

To understand the factors that determine the energy consumption of a drone, we carried out the following experiments for obtaining empirical data in the rural areas, where the drone can fly in a straight path without obstacles:

- 1) *Impact of Motion*: The motions of a drone can be divided into three types: hovering, horizontal moving and vertical moving. We study the energy consumption of the test drone in each motion type.
- 2) *Impact of Weight*: Typical drones can carry extra payloads, such as camera equipment or parcels. We study the impact of different weights of payloads.
- 3) *Impact of Wind*: The major environmental factor that affects the drone is wind, including wind direction and speed. Wind may benefit the energy consumption in some cases, as well as incurring resistance to the movement in other cases. We study the energy consumption of the test drone in various wind conditions.

The experimental results are described as follows.

1) *Impact of Motion*: To study the energy consumption of motions of the drone, we conducted three experiments. The battery power, barometer and GPS location, and speed data are collected in each experiment to analyze the motions of the test drone.

Fig. 2 depicts the recorded data traces of the three experiments. We discuss the observations as following:

- *Experiment 1*: The test drone hovers in the air without any movement in this experiment. Note that the drone may slightly drift around the takeoff location due to deviation error of GPS modules. We filter the speed data that is smaller than 0.5 m/s. This experiment shows the baseline power consumption of a flying drone. From the recorded data, we observe that the drone can maintain a sufficiently

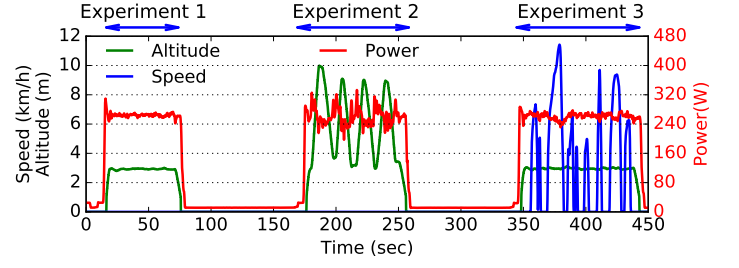


Fig. 2: Motion and battery power consumption of the test drone.

steady flying altitude and the power consumption is steady.

- *Experiment 2*: The test drone ascends and descends repeatedly in this experiment. The barometer data shows the altitude of the drone. Time series data allow us to compute the vertical acceleration and speed of the drone. We observe larger power fluctuations due to repeatedly vertical movements. The power consumption increases, when the drone ascends.
- *Experiment 3*: The test drone moves horizontally without altering its altitude in this experiment. The GPS data comprises of speed and course angle of the drone. We also gathered average wind speed and direction using a wind speed meter during the experiment. We observe smaller power fluctuations due to horizontal movements. We also observe the idle power consumption of the drone between the two experiments.

2) *Impact of Weights*: One of the practical purposes of drones is to deliver payloads, and hence, the total weight of a drone varies as the payload it carries. We carried out several experiments with different weights of payloads on the drone to obtain empirical data. Three different weights are tested on the drone. The drone is set to hover in the air without any movement to obtain the corresponding baseline power consumption.

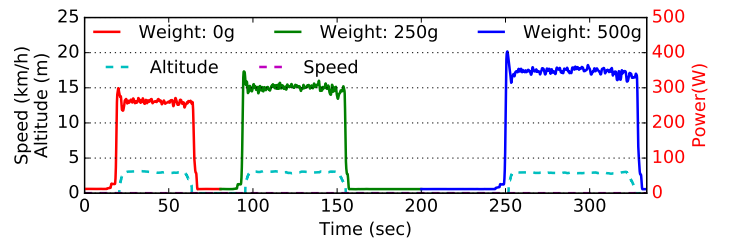


Fig. 3: Battery power consumption of the test drone with different payload weights.

Fig. 3 depicts the battery power consumption of the test drone carrying three different weights. We observe that the power consumption increases when the weight of payload increases. The weight limit of payload depends on the thrusts that the motors can produce. Note that the maximum payload weight is 500g for 3DR Solo drone.

3) *Impact of Wind*: Wind condition is a major environmental factor to the power consumption of a drone. We conducted

several experiments under different wind conditions: *headwind* by flying against the direction of wind, and *tailwind* by flying along the direction of wind. The experiments are carried out at the same location but on different days with different wind conditions. The wind directions and average speeds are measured using a wind speed meter for each experiment. Once the wind direction is determined, the drone is set to fly into a headwind or tailwind at maximum speed (18 km/h).

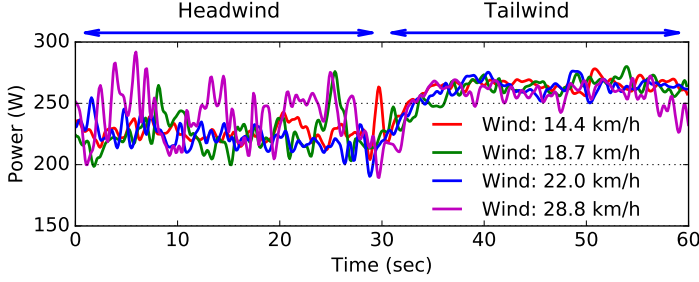


Fig. 4: Battery power consumption of the test drone under different wind conditions.

Fig. 4 depicts the battery power consumption of the drone under different wind conditions. We observe smaller power consumption when flying into headwind, which is due to the increasing thrust by *translational lift*, when the drone moves from hovering to forward flight. When flying into a headwind, translational lift increases due to the relative airflow over the propellers increases, resulting in less power consumption to hover the drone [13]. However, when the wind speed exceeds a certain limit, the aerodynamic drag may outweighs the benefit of translational lift. In our setting, the drone speed is relatively slow, even at maximum speed. Hence, flying into a headwind is likely more energy-efficient.

### B. Regression Model of Energy Consumption for Drone

Since drones are electric vehicles, we can apply the methodology from the literature of electric vehicles to model the energy consumption of drones. There are two main types of energy consumption models of a drone:

- **White-box Model:** A straightforward approach is to employ a white-box microscopic behavior model for each drone that comprehensively characterizes the motor performance, aerodynamic environment, and battery systems. However, such a white-box model requires a large amount of data for calibration and detailed knowledge specific to a particular drone. For example, the aerodynamic parameters such as propeller efficiencies, motor efficiencies and drag coefficients are difficult to obtain accurately without resorting to sophisticated experimental setups like wind tunnel.
- **Blackbox Model:** A blackbox approach is more desirable that requires minimal knowledge of vehicle model with only a small set of measurable variables and parameters of the drone. In the subsequent sections, a blackbox model of energy consumption of drone will be utilized for tour planning with recharging optimization. The advantage of blackbox model is that it is obtained from

simple data measurements without using sophisticated experimental setups.

This section describes a linear blackbox model of energy consumption for drones that has been used extensively in the literature of electric vehicles [14], [15], [7], [16], [17], [18].

Let the estimated battery power consumption of a drone be  $\hat{P}$ , which is estimated by a number of measurement parameters in the following linear equation:

$$\hat{P} = \begin{bmatrix} \beta_1 \\ \beta_2 \\ \beta_3 \end{bmatrix}^T \begin{bmatrix} \|\vec{v}_{xy}\| \\ \|\vec{a}_{xy}\| \\ \|\vec{v}_{xy}\| \|\vec{a}_{xy}\| \end{bmatrix} + \begin{bmatrix} \beta_4 \\ \beta_5 \\ \beta_6 \end{bmatrix}^T \begin{bmatrix} \|\vec{v}_z\| \\ \|\vec{a}_z\| \\ \|\vec{v}_z\| \|\vec{a}_z\| \end{bmatrix} + \begin{bmatrix} \beta_7 \\ \beta_8 \\ \beta_9 \end{bmatrix}^T \begin{bmatrix} m \\ \vec{v}_{xy} \cdot \vec{w}_{xy} \\ 1 \end{bmatrix} \quad (1)$$

where

- $\vec{v}_{xy}$  and  $\vec{a}_{xy}$  are the speed and acceleration vectors describing the horizontal movement of the drone.
- $\vec{v}_z$  and  $\vec{a}_z$  are the speed and acceleration vectors describing the vertical movement of the drone.
- $m$  is the weight of payload.
- $\vec{w}_{xy}$  is the vector of wind movement in the horizontal surface.
- $\beta_1, \dots, \beta_9$  are the coefficients, and  $\|\vec{v}\|$  denotes the magnitude of a vector.

The coefficients  $\beta_1, \dots, \beta_9$  can be estimated by the standard regression method, if sufficient measurement data is collected.

Assuming the uniform conditions (e.g., speed, wind) within a period of duration  $D$ , the total energy consumption of the drone is estimated by  $\hat{P} \cdot D$ .

### C. Evaluation of Regression Model

To evaluate the accuracy of the energy consumption regression model, we conducted experiments to collect measurement data to estimate the corresponding coefficients. The test drone was programmed to first fly vertical movements, then flying into a headwind and a tailwind with different weights of payloads. The drone maintains its altitude during the horizontal flight. We conducted experiments under simple conditions, where the drone ascends from the source until reaching the desired altitude and then flies directly to the destination without changing its altitude. But the experiments are sufficiently representative of other conditions.

Fig. 5a depicts the collected data of our experiments. We tested 3 different weights of payloads under similar flight paths operations. We obtain the estimated power consumption using the regression model, and compare it to the measured power consumption shown in Fig. 5b. We observe that the estimation is close to the actual measurement data. We integrate power over time to obtain the energy consumption of the drone in Fig. 5c. The error of estimation of energy consumption in the experiments is within 0.4%, which shows relatively good accuracy of our regression model of energy consumption for the test drone.

## IV. FLIGHT TOUR PLANNING WITH RECHARGING

In this paper, we utilize the energy consumption model for drone from the last section to study a joint problem of



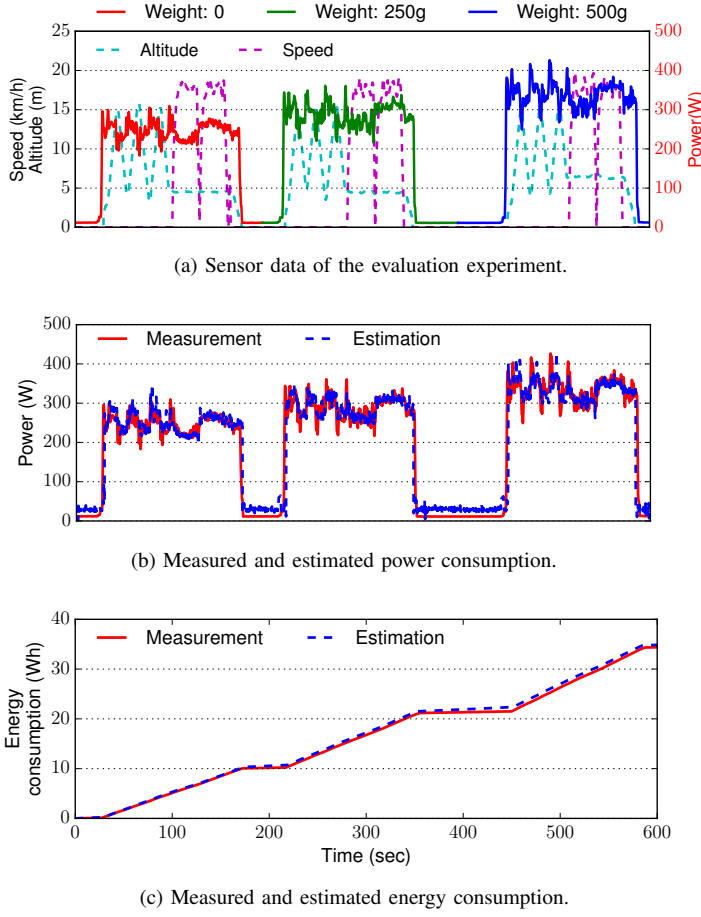


Fig. 5: Evaluation of the energy consumption regression model of the test drone.

flight tour planning with recharging optimization for battery-operated autonomous drones. The objective is to complete a tour mission for a set of sites of interest in the shortest time. We consider a variable number of charging stations to allow recharging of drones intermediately. This problem naturally captures diverse applications of delivery and remote operations by drones. We provide efficient algorithms to determine the solutions in an intelligent drone management system.

#### A. Model and Formulation

We consider a set of sites of interest  $\mathcal{S}$  that a drone needs to visit (e.g., drop-off locations of parcels, or sites for surveillance), and a set of charging stations  $\mathcal{C}$  that a drone can receive recharging. The base location of drones is denoted by  $v_0$ . The problem is to find a flight plan (a sequence of locations in  $\mathcal{S}$  and  $\mathcal{C}$ ), such that the drone can visit all sites in  $\mathcal{S}$ , starting and terminating at  $v_0$ , with the objective of minimizing the total trip time, while maintaining the state-of-charge (SoC) within the operational range.

Note that the flight path between a pair of locations may be affected by weather conditions and no-fly zone restriction. Given a pair of locations  $(u, v)$ , we denote the designated flight path by  $\ell(u, v)$ , and the flight time by  $\tau(u, v)$ . Let

$f(\ell(u, v), \tau(u, v))$  be the required energy consumption<sup>1</sup> for the drone flying along  $\ell(u, v)$  within flight time  $\tau(u, v)$ . That is,  $f(\cdot, \cdot)$  is an increasing function that maps the combination of flight path  $\ell(u, v)$  and flight time  $\tau(u, v)$  to the required amount of energy.

Let  $V \triangleq \mathcal{S} \cup \mathcal{C} \cup \{v_0\}$ . If the drone flies between two sites  $u, v \in V$ , then it consumes an amount of energy from the battery denoted by  $\eta_d f(u, v)$ . If the drone flies to a charging station  $u \in \mathcal{C}$ , it can recharge its battery by an amount of energy denoted by  $\eta_c b(u)$ .  $\eta_c \leq 1$  and  $\eta_d \geq 1$  are the charging and discharging efficiency coefficients. When recharging its battery at  $u$ , let the incurred charging time be  $\tau_c(b(u))$ . We denote the flight plan by  $\mathcal{T}$ , which consists of a sequence of locations in  $\mathcal{T} \subseteq \mathcal{S} \cup \mathcal{C} \cup \{v_0\}$ , and denote  $k$ -th location by  $\mathcal{T}_k$ . We require  $\mathcal{T}_1 = \mathcal{T}_{|\mathcal{T}|} = v_0$ . The objective is to find a flight plan that minimizes the total trip time, consisting of the travel time plus the charging time. See an illustration of a flight plan with recharging for a drone in Fig. 6.

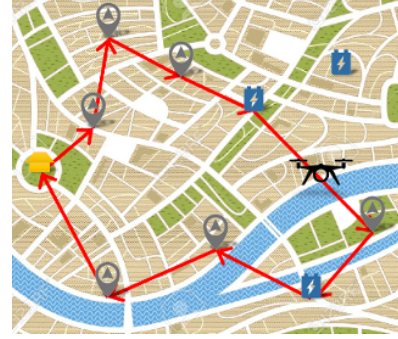


Fig. 6: A flight plan with recharging for a drone.

This problem can be formally formulated as follows. Let  $x_k$  be the SoC when reaching the  $k$ -th location in the flight plan. We require the SoC lying within feasible range  $[\underline{B}, \overline{B}]$ . The lower bound of SoC  $\underline{B}$  ensures sufficient residual energy for the drone to return to the base, in case of emergency. With the above notations, the drone flight plan optimization problem (DFP) is formulated as follows.

$$(\text{DFP}) \min_{\mathcal{T}, b(\cdot), x} \sum_{k=1}^{|\mathcal{T}|-1} \tau(\mathcal{T}_k, \mathcal{T}_{k+1}) + \sum_{k=1: \mathcal{T}_k \in \mathcal{C}}^{\mathcal{T}} \tau_c(b(\mathcal{T}_k)) \quad (2)$$

subject to

$$\mathcal{T}_1 = \mathcal{T}_{|\mathcal{T}|} = v_0 \quad (3)$$

$$\mathcal{S} \subseteq \mathcal{T} \subseteq \mathcal{S} \cup \mathcal{C} \cup \{v_0\} \quad (4)$$

$$x_k = \begin{cases} x_{k-1} - \eta_d f(\ell(\mathcal{T}_k, \mathcal{T}_{k+1}), \tau(\mathcal{T}_k, \mathcal{T}_{k+1})), & \text{if } \mathcal{T}_k \in \mathcal{S} \\ x_{k-1} + \eta_c b(\mathcal{T}_{k+1}) - \eta_d f(\ell(\mathcal{T}_k, \mathcal{T}_{k+1}), \tau(\mathcal{T}_k, \mathcal{T}_{k+1})), & \text{if } \mathcal{T}_k \in \mathcal{C} \end{cases} \quad (5)$$

$$\underline{B} \leq x_k \leq \overline{B} \quad (6)$$

<sup>1</sup>We assume a simple flight path, such that the drone first ascends vertically to a desired altitude, and then travels in a straight path, and finally descends to the destination vertically.

In general, the flight plan optimization with recharging problem can be solved by optimization using drone flight historic data. We can extend this problem to further incorporate a variety of further factors for practical flight plan optimization, such as restrictions of no-fly zones and attitude, and wind speed forecast information. Users can also specify further goals, such as deadline of completion and maximum payload weight. An efficient optimization algorithm is derived to compute an optimal flight path to meet the users' specified goals (e.g., traversing all targeted sites of surveillance, and returning to the base).

### B. Case with Uniform Drone Speed & Steady Wind Condition

Suppose that the horizontal speed of the drone is a uniform constant under steady wind condition, which will be generalized in Sec. IV-C. The travel time  $\tau(u, v)$  between two sites  $u, v \in \mathcal{V}$  is proportional to the length of flight path  $\ell(u, v)$ , denoted by  $d(u, v)$ . Our regression model of energy consumption for drone in Sec. III implies that the function  $f(\ell(u, v), \tau(u, v))$  is linear in the distance  $d(u, v)$ , and that the charging time  $\tau_c(b(u))$  is linear in the amount of recharged energy  $b(u)$ . Thus, we may assume the following

$$\begin{aligned}\tau(u, v) &= c_a d(u, v), & \tau_c(b(u)) &= c_b b(u), \\ f(\ell(u, v), \tau(u, v)) &= c_f d(u, v),\end{aligned}$$

for some constants  $c_a, c_b, c_f(u, v) > 0$ . Note that we allow  $c_f(u, v)$  to depend on the edge  $(u, v)$ ; this could be useful to model the non-uniform environment for each  $\ell(u, v)$ , for instance, paths where stronger wind is expected should have larger constants  $c_f(u, v)$ . In this paper, we consider mostly long-distance trips (e.g., 2-3 km) in this paper, for which the vertical landing and take-off operations usually constitute a small part of the whole flight, and consume only a small percentage of the total energy (e.g.,  $< 1\%$ ). For clarity of presentation, we assume that the energy consumption of landing and take-off operations is implicitly captured by  $c_f(u, v)d(u, v)$ , though our results can be easily extended to consider that explicitly.

Define  $\underline{c}_f \triangleq \min_{(u,v)} c_f(u, v)$  and  $\bar{c}_f \triangleq \max_{(u,v)} c_f(u, v)$ .

Under these assumptions, we may also assume that the total contribution of the charging time  $\sum_{k=1}^{|\mathcal{T}|-1} \tau_c(b(\mathcal{T}_k))$ , in the optimal tour  $\mathcal{T}$ , is proportional to the total travel time  $\sum_{k=1}^{|\mathcal{T}|-1} \tau(\mathcal{T}_k, \mathcal{T}_{k+1})$ , as the following lemma suggests.

**Lemma 1:** In an optimal flight plan  $(\mathcal{T}, b(\cdot))$ , we have<sup>2</sup>

$$\sum_{k=1}^{|\mathcal{T}|-1} \tau(\mathcal{T}_k, \mathcal{T}_{k+1}) + \sum_{k=1}^{|\mathcal{T}|} \tau_c(b(\mathcal{T}_k)) \in [\underline{c}, \bar{c}]d(\mathcal{T}) + c',$$

where either  $\underline{c} = \bar{c} = c_a$  and  $c' = 0$ , or  $\underline{c} = c_a + \underline{c}_f c_b \frac{\eta_d}{\eta_c}$ ,  $\bar{c} = c_a + \bar{c}_f c_b \frac{\eta_d}{\eta_c}$ , and  $c' = \frac{c_b}{\eta_c}(\bar{B} - x_0)$ .  $x_0$  is the initial SoC at  $v_0$ , and  $d(\mathcal{T}) \triangleq \sum_{k=1}^{|\mathcal{T}|-1} d(\mathcal{T}_k, \mathcal{T}_{k+1})$ .

*Proof:* See the Appendix. ■

The proof of Lemma 1 also implies the following.

<sup>2</sup>For brevity, we use the notation:  $[\underline{c}, \bar{c}]d(\mathcal{T}) + c'$  to mean the interval  $[\underline{c} \cdot d(\mathcal{T}) + c', \bar{c} \cdot d(\mathcal{T}) + c']$

**Corollary 1:** Given any feasible flight plan  $(\mathcal{T}, b(\cdot))$ , there is another feasible flight plan  $(\mathcal{T}, b'(\cdot))$  such that

$$\sum_{k=1: \mathcal{T}_k \in \mathcal{C}}^{|\mathcal{T}|} b'(\mathcal{T}_k) \leq \frac{\bar{B} - x_0}{\eta_c} + \frac{\bar{c}_f \eta_d}{\eta_c} \sum_{k=1}^{|\mathcal{T}|-1} d(\mathcal{T}_k, \mathcal{T}_{k+1}).$$

Such a plan  $(\mathcal{T}, b'(\cdot))$  can be found in  $O(|V|)$  time.

*Proof:* Algorithm Fix-charge implements the argument used in the proof of Lemma 1. ■

Lemma 1 allows us to reduce the problem to the so-called *tour gas station problem* in [10]. Up to several constants, the simplified formulation (SDFP) is as follows.

$$(\text{SDFP}) \min_{\mathcal{T}, x} \sum_{k=1}^{|\mathcal{T}|-1} d'(\mathcal{T}_k, \mathcal{T}_{k+1}) \quad (7)$$

$$\text{subject to } \mathcal{T}_1 = \mathcal{T}_{|\mathcal{T}|} = v_0 \quad (8)$$

$$\mathcal{S} \subseteq \mathcal{T} \subseteq \mathcal{S} \cup \mathcal{C} \cup \{v_0\} \quad (9)$$

$$x_k = \begin{cases} x_{k-1} - \eta_d d'(\mathcal{T}_k, \mathcal{T}_{k+1}), & \text{if } \mathcal{T}_k \in \mathcal{S} \\ \bar{B}, & \text{if } \mathcal{T}_k \in \mathcal{C} \end{cases} \quad (10)$$

$$\bar{B} \leq x_k \leq \bar{B} \quad (11)$$

Note that we assume in the above formulation that the SoC is brought to its maximum at each charging station. Once we obtain a tour under this assumption, it can be turned into a flight plan with the minimal charging requirements using Corollary 1.

Let  $V \triangleq \mathcal{S} \cup \mathcal{C} \cup \{v_0\}$ . We interpret  $\{c_f(u, v)d(u, v)\}_{u,v}$  as edge lengths on a weighted undirected graph  $G_0 = (V, \binom{V}{2})$  and compute the pairwise shortest distances  $\{d'(u, v)\}_{u,v}$  on this graph. For  $u \in V$ , let  $d'_u \triangleq \min_{v \in \mathcal{D}} d'(u, v)$  and  $g_u \triangleq \arg\min_{v \in \mathcal{D}} d'(u, v)$ .

Let  $U \triangleq \frac{\bar{B} - \bar{B}}{\eta_d}$ . Following [10], we make the technical assumption that for every  $u \in \mathcal{S} \setminus \{v_0\}$  there is  $v \in \mathcal{C}$  such that  $d(u, v) \leq \alpha \frac{U}{2}$ , where  $\alpha \in [0, 1]$ . This assumption can be justified (for  $\alpha = 1$ ) as follows. For a location  $u \in \mathcal{S} \setminus \{v_0\}$ , if every  $v \in \mathcal{C}$  is at distance greater than  $\frac{U}{2}$ , then there is no way to visit  $u$  in the tour without getting the battery level below  $\bar{B}$  (as the SoC would drop below  $\bar{B} - \eta_d U = \bar{B}$ ).

The main algorithm to solve SDFP is Find-plan $[V, d]$ , which calls three other procedures:

- **Init-distances** $[V, d', u, v]$ : This provides a lower bound for the optimal solution. Namely, it finds for every pair of locations  $u, v \in V$ , the minimum possible distance  $d(u, v)$ , and the corresponding shortest path  $\mathcal{P}(u, v)$  to go from  $u$  to  $v$  without going out of the operational range of the battery. Note that if  $d'(u, v) \leq U - d'_u - d'_v$ , then the drone can go directly from  $u$  to  $v$ . (Indeed, starting with SoC  $= \bar{B}$  at  $g_u$ , then the drone reaches  $u$  with SoC  $\bar{B} - \eta_d d'_u$ , and then it travels directly from  $u$  to  $v$  causing the SoC to drop to  $\bar{B} - \eta_d (d'_u + d'(u, v)) = \bar{B} + \eta_d (U - d'_u - d'(u, v)) \geq \bar{B} + \eta_d d'_v$  at  $v$ . So there is enough battery at  $v$  to reach  $g_v$ .) Otherwise, at best (in the optimal solution), the drone can reach  $u$  with SoC at most  $\bar{B} - \eta_d d'_u$ , then it can go through some charging stations (only if the distance  $d'$  between two successive such stations is at most  $U$ ), then, from the last station, it

Algorithm 1. Fix-charge $[\mathcal{T}, b(\cdot)]$	Algorithm 3. Init-distances $[V, d', u, v]$	Algorithm 4. Fix-tour $[G, \mathcal{T}_0]$
1: Let $\mathcal{T}_{i_1}, \dots, \mathcal{T}_{i_r}$ be the charging stations, in the order they appear on $\mathcal{T}$ 2: <b>for</b> $j = 0, 1, \dots, r$ <b>do</b> 3: $D_j = \eta_d \sum_{k=i_j}^{i_{j+1}-1} c_f(\mathcal{T}_k, \mathcal{T}_{k+1})d(\mathcal{T}_k, \mathcal{T}_{k+1})$ 4: <b>end for</b> 5: <b>for</b> $j = 1, \dots, r$ <b>do</b> 6: $B_j \triangleq \eta_c \sum_{k=1}^j b(\mathcal{T}_{i_k})$ 7: <b>end for</b> 8: <b>for</b> $j = r$ <b>downto</b> 1 <b>do</b> 9: $b'(\mathcal{T}_{i_j}) = \max\{0, \frac{1}{\eta_c}(\underline{B} - x_0 + \sum_{k=0}^r D_k - \sum_{k=1}^{j-1} B_k)\}$ 10: <b>if</b> $b'(\mathcal{T}_{i_j}) > 0$ <b>then</b> 11: <b>exit</b> 12: <b>end if</b> 13: <b>end for</b> 14: <b>return</b> $b'(\cdot)$	1: <b>if</b> $d'(u, v) \leq U - d'_u - d'_v$ <b>then</b> 2: $\tilde{d}'(u, v) \leftarrow d'(u, v), \mathcal{P}(u, v) \leftarrow \{(u, v)\}$ 3: <b>return</b> $(\tilde{d}(u, v), \mathcal{P}(u, v))$ 4: <b>else</b> 5:     Construct a weighted undirected graph 6: $G = (\mathcal{C} \cup \{u, v\}, E; w)$ where 7: $E \triangleq \left\{ \begin{aligned} &\{u, z\} : z \in \mathcal{C}, d'(u, z) \leq U - d'_u \end{aligned} \right\} \cup$ 8: $\left\{ \begin{aligned} &\{v, z\} : z \in \mathcal{C}, d'(v, z) \leq U - d'_v \end{aligned} \right\} \cup$ 9: $\left\{ \begin{aligned} &\{z, z'\} : z, z' \in \mathcal{C}, d'(z, z') \leq U \end{aligned} \right\}$ 10:     and $w(z, z') \triangleq d'(z, z')$ for all $z, z' \in \mathcal{C} \cup \{u, v\}$ 11: $\mathcal{P}(u, v) \leftarrow$ shortest path between $u$ and $v$ in $G$ (with edge lengths $w$ ) 12: $\tilde{d}(u, v) \leftarrow$ length of $\mathcal{P}(u, v)$ 13: <b>return</b> $(\tilde{d}(u, v), \mathcal{P}(u, v))$ 14: <b>end if</b>	1: $\mathcal{T} \leftarrow \emptyset$ 2: <b>for</b> each $(u, v)$ in $\mathcal{T}_0$ <b>do</b> 3:     Add $\mathcal{P}(u, v)$ to $\mathcal{T}$ 4: <b>end for</b> 5: Add to $\mathcal{T}$ a set of sub-tours 6: $\{(u, g_u), (g_u, u) : u \in V\}$ 7: <b>for</b> $u \in V$ <b>do</b> 8: <b>if</b> $\mathcal{T} \setminus \{(u, g_u), (g_u, u)\}$ is feasible <b>then</b> 9: $\mathcal{T} \leftarrow \mathcal{T} \setminus \{(u, g_u), (g_u, u)\}$ 10: <b>end if</b> 11: <b>end for</b> 12: <b>return</b> $\mathcal{T}$

has to reach  $v$  such that the SoC at  $v$  is at least  $\underline{B} + \eta_d d'_v$  (so that there is enough battery to reach  $g_v$ ). In particular, the distance from  $u$  to the first charging station on this path should be at most  $U - d'_u$ ; similarly, the distance from the last station on the path to  $v$  should be at most  $U - d'_v$ . This explains the definition of the graph  $G$  in line 5 of the procedure.

- **Fix-tour $[G, \mathcal{T}_0]$** : starting from the tour  $\mathcal{T}_0$  obtained using the (modified) Christofides algorithm with respect to the weights  $\tilde{d}$ , this procedure reconstructs a feasible tour  $\mathcal{T}$  for problem (SDFP). It first replaces each edge  $(u, v)$  in the tour by the corresponding path  $\mathcal{P}(u, v)$ . Since the resulting tour maybe still infeasible, the procedure adds to every site a round trip to the closest charging station. Finally, the added stations are dropped one by one in a greedy way as long as feasibility is maintained.
- **Fix-charge $[\mathcal{T}, b(\cdot)]$** : Starting from the flight plan  $(\mathcal{T}, b(\cdot))$  constructed after calling procedure **Fix-tour $[G, \mathcal{T}_0]$** , this procedure finds a minimal amount of recharged energy, according to Corollary 1.

The main algorithm is a modification of Christofides Algorithm [11], which finds a minimum spanning tree with respect to the weights  $\tilde{d}$  and then a minimum weight perfect matching  $M$  on the odd vertices of  $T$ . The edges of  $T$  and  $M$  define an Eulerian graph from which an Eulerian tour  $\mathcal{T}_0$  can be obtained in linear time. This Eulerian tour is passed to the procedure **Fix-tour** to convert it to a feasible tour  $\mathcal{T}$  which might use a non-optimal charging function  $b(\cdot)$ . The resulting plan  $(\mathcal{T}, b(\cdot))$  is further passed to procedure **Fix-charge** to minimize the charging requirement with respect to the tour  $\mathcal{T}$ .

Let  $\text{OPT}_{\text{DFP}}$  and  $\text{OPT}_{\text{SDFP}}$  be the optimal solutions of problems (DFP) and (SDFP), respectively.

**Lemma 2 ([10]):** The tour  $\mathcal{T}$  returned by Algorithm **Find-plan $[V, d]$**  has cost  $d'(\mathcal{T}) \leq \frac{3}{2} \left( \frac{1+\alpha}{1-\alpha} \right) \text{OPT}_{\text{SDFP}}$ .

For convenience of notation, for a flight plan  $(\mathcal{T}, b(\cdot))$  let us write  $\tau(\mathcal{T}) \triangleq \sum_{k=1}^{|\mathcal{T}|-1} \tau(\mathcal{T}_k, \mathcal{T}_{k+1})$  and  $b(\mathcal{T}) \triangleq \sum_{k=1}^{|\mathcal{T}|} \tau_{\mathcal{T}_k \in \mathcal{C}} \tau_c(b(\mathcal{T}_k))$ . The following theorem establishes that Algorithm **Find-plan $[V, d]$**  has an asymptotic constant-factor approximation guarantee, in the linear function case.

**Theorem 2:** The flight plan  $(\mathcal{T}, b'(\cdot))$  returned by Algorithm

Algorithm 2. Find-plan $[V, d]$
1: Compute all pairwise shortest distances $\{d'(u, v)\}_{u, v}$ on the weighted undirected graph $G_0 = (V, \binom{V}{2})$ 2: <b>for</b> each $u, v \in V$ <b>do</b> 3: $(\tilde{d}(u, v), \mathcal{P}(u, v)) \leftarrow \text{Init-distances}[V, d', u, v]$ 4: <b>end for</b> 5: Consider the weighted undirected graph $G = (V, E; \tilde{d})$ where $E = \binom{V}{2}$ 6: Find a minimum spanning tree $T = (V, E_T)$ in $G$ 7: $V_0 \leftarrow$ find the set of odd degree vertices in $T$ 8: Find a minimum-weight perfect matching $M = (V_0, E_M)$ in the graph $(V_0, E; \tilde{d})$ 9: $\mathcal{T}_0 \leftarrow$ find an Eulerian tour in the graph $(V, E_T \cup E_M)$ 10: $\mathcal{T} \leftarrow \text{Fix-tour}[G, \mathcal{T}_0]$ 11: $b'(\cdot) \leftarrow \text{Fix-charge}[\mathcal{T}, b(\cdot)]$ 12: <b>return</b> $(\mathcal{T}, b'(\cdot))$

**Find-plan $[V, d]$**  has cost

$$\tau(\mathcal{T}) + \tau_c(b(\mathcal{T})) = O(\text{OPT}_{\text{DFP}}) + O(1).$$

*Proof:* See the Appendix. ■

### C. Extensions

In this section, we present extensions to above algorithms to obtain heuristics for more practical scenarios.

1) *Wind Uncertainty:* Under steady wind condition, we assume in the above algorithms that  $c_f(u, v)$  is a constant that depends on the designated path between sites  $u$  and  $v$ . In practice, there is sometimes uncertainty in the wind condition. Often, the wind varies as the drone flies. Hence, this also depends on the wind expected on this path, so it should be actually  $c_f(u, v, w)$ , where  $w$  is the wind vector that assumes values in uncertain domain  $w \in W$ . For example, we predict the wind speed will be in the range  $[\underline{w}, \overline{w}]$  and the orientation in the range  $[\underline{\theta}_w, \overline{\theta}_w]$ . To account for the uncertainty, we proceed conservatively in our algorithm; we may replace  $c_f(u, v)$  by  $\bar{c}_f(u, v) = \max_{w \in W} c_f(u, v, w)$ .

2) *Variable Drone Speed:* We consider a scenario, where we can vary the drone speed uniformly at all designated paths in  $V$ . In this case, we will run our algorithms sequentially with an increasing drone speed at each round, until the algorithms can not return a feasible solution (because higher drone speed may result in insufficient battery to reach some sites). Then we will enumerate all the optimal solutions in all the rounds to find the best solution with the lowest total travel time.

## V. CASE STUDIES

We implemented the algorithms and evaluate the results of tour planning with recharging optimization for the test drone in several case studies in this section.

### A. Setup

We consider a scenario with four sites of interest, and four charging stations. The drone is programmed to begin its mission from the base. Fig. 7 depicts the geographical locations of the sites (as black points), charging stations (as blue squares) and the base (as magenta triangle). This case studies are based on the real locations of a suburban community.

- 1) *Simulation 1*: We simulated four cases using the energy consumption model of 3DR Solo drone under different wind and payload conditions. We consider the standard 3DR Solo drone which is equipped with 70 Wh battery capacity in the first two cases. A mild wind condition with average wind speed of 18 km/h is simulated in all cases. Then we double the battery capacity with the same wind condition in another two cases. Since the battery capacity is doubled, extra weight is added to the drone. One battery weights 500g. The parameters of all the cases are summarized in Table II.
- 2) *Simulation 2*: We consider uncertainty of wind condition. The wind speed and orientation vary within a certain range. The wind speed varies from 0 to 21 km/h in four discrete scales, while the wind orientation varies from  $0^\circ$  to  $360^\circ$  in four discrete scales.

The cases of Simulation 1 are denoted by  $S_1C_1$  to  $S_1C_4$ , and the cases of Simulation 2 are denoted by  $S_2C_1$  to  $S_2C_4$ .

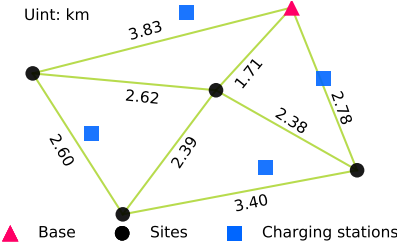


Fig. 7: Geographical locations of the sites, charging stations and base.

Case	Battery (Wh)	$\ \vec{w}_{xy}\ $ 20 (km/h)	$m$ (g)
1	70	South	0
2	70	North-East	0
3	140	South	500
4	140	North-East	500

TABLE II: Parameters of setup.

### B. Results and Discussion

1) *Simulation 1*: Fig. 8 visualizes the results of Simulation 1. The numbers indicate the path order of the drone. The colors represent the SoC of battery. The wind orientations are displayed on the upper-left corners.

We plot the travel time and energy consumption of Simulation 1 in Fig. 10. We normalize the travel time and energy consumption by the results of  $S_1C_1$  (i.e., the lowest travel time and energy consumption), as listed in Table III. There are two observations:

- The north-east wind causes higher energy consumption than that by south wind. Besides, higher travel time is observed due to longer charging time.
- Increasing battery capacity for 3DR Solo drone does not help to reduce the travel time. We observe that even the flying time in  $S_1C_3$  is the shortest, it takes more time to charge since the drone becomes heavier by carrying extra weight for the battery, which results in longer travel time.

	$S_1C_1$	$S_1C_2$	$S_1C_3$	$S_1C_4$
Travel Time	1	1.07	1.15	1.20
Energy Consumption	1	1.07	1.24	1.48

TABLE III: Comparisons of results

2) *Simulation 2*: Fig. 9 visualizes the results of Simulation 2. The numbers indicate the path order for the drone. We represent the ranges of wind speeds and orientations as the shaded areas on the upper-left corners. We plot the travel time and energy consumption of Simulation 2 in Fig. 11.

The energy consumption of  $S_1C_1$  is the result without uncertain wind condition for the 3DR solo drone with 70 Wh battery. In Simulation 2, we study if a solution can be obtained in the presence of uncertainty of wind condition. We gradually increase the uncertainty from  $S_2C_1$  to  $S_2C_4$ . For example, in  $S_2C_1$  the wind speed varies from 9 to 12 km/h and orientation varies from  $-45^\circ$  to  $45^\circ$ . We observe that the energy consumption increases as the uncertainty of wind condition increases in Fig. 11. The energy consumption of the worst uncertainty is in  $S_2C_4$ , in which the drone may always fly into a tailwind.  $S_2C_4$  provides the most conservative result.

## VI. INTELLIGENT DRONE MANAGEMENT SYSTEM

We implemented our algorithms in an intelligent drone management system. The user interface is depicted in Fig 12. The user interface allows the users to specify individual goals and to visualize the computed flight plan. The system connects to the cloud computing server, which uses the desired locations from the user and computes the optimal flight plan. The drone is programmed to follow the flight plan computed by the server. Furthermore, a dynamic tracking system of drone using on-board sensors, including GPS location, video feed, SoC, and flight status, is utilized to monitor the real-time flight status of drones. If abnormal measurements are detected, for example, the reported sensor measurements deviate from estimated value by flight tour planning, then real-time re-computation will be performed to find the minimum adjustment to the previously computed flight plan. The user can abort the mission anytime by clicking the button on the system. We remark that multiple drones can also be tracked simultaneously.

## VII. CONCLUSION

Intelligent drone management system is important for practical applications of drones. This paper provides multiple contributions for automated battery-operated drone management systems, including an empirical study to model the battery performance of drones, considering various flight scenarios,



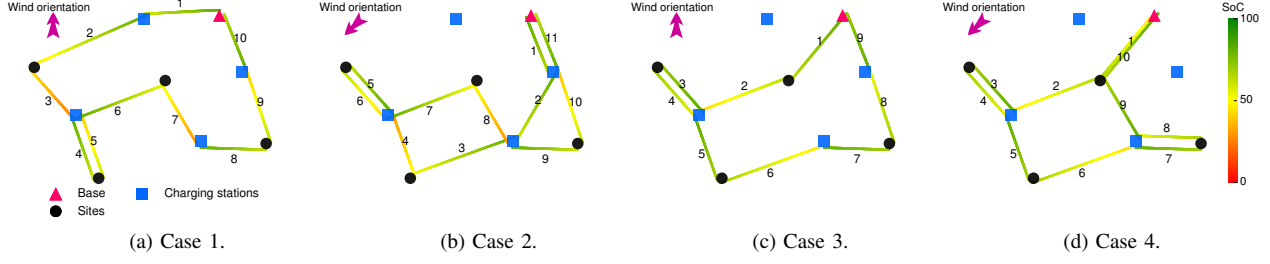


Fig. 8: Visualized results of Simulation 1.

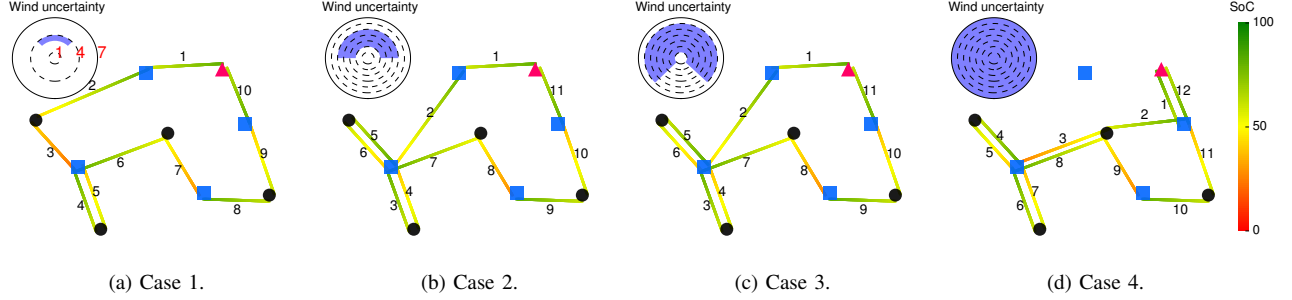


Fig. 9: Visualized results of Simulation 2.

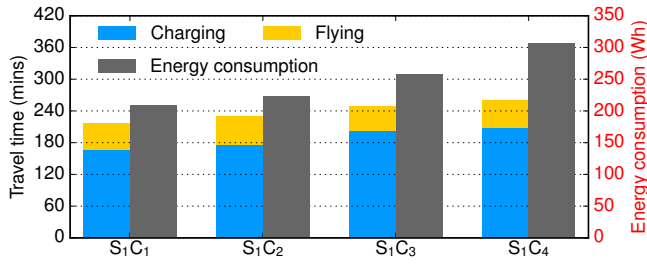


Fig. 10: Results of Simulation 1.

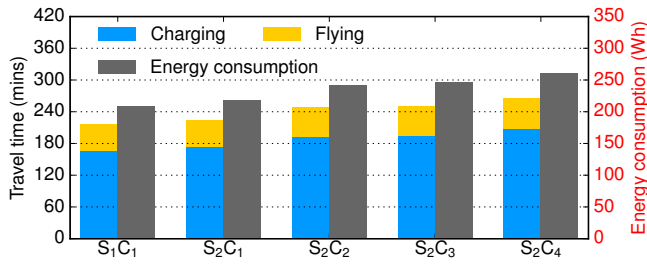


Fig. 11: Results of Simulation 2.

a study of flight tour planning with recharging optimization for drones that captures diverse applications of delivery and remote operations by drones, and a management system implementation. In the future, we will extend to incorporate a variety of further factors, such as restrictions of no-fly zones and attitude, and wind speed forecast. Users may also be to specify further goals, such as deadline of completion and maximum payload weight.

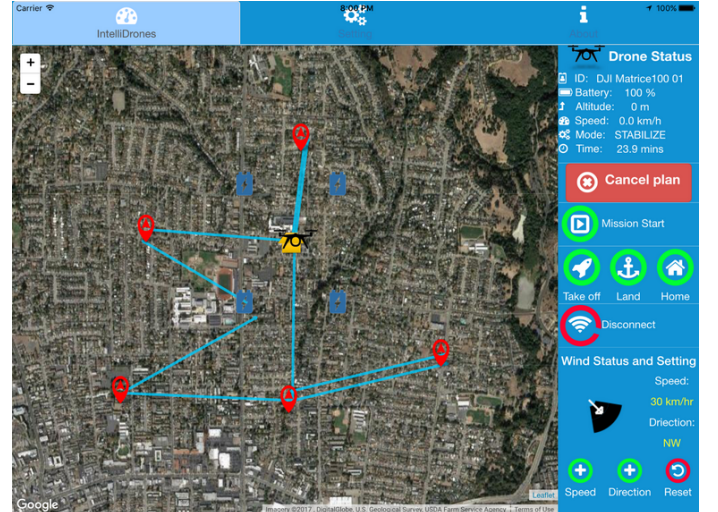


Fig. 12: Interface of intelligent drone management system.

## REFERENCES

- [1] G. Bensinger and L. Stevens, "Amazon's newest ambition: Competing directly with ups and fedex," in *The Wall Street Journal*, Sep 2016. [Online]. Available: <http://www.wsj.com/articles/amazons-newest-ambitioncompeting-directly-with-ups-and-fedex-1474994758>
- [2] "Welcome to Larry Page's secret flying-car factories," in *Bloomberg Businessweek*, Jun 2016. [Online]. Available: <https://www.bloomberg.com/news/articles/2016-06-09/welcome-to-larry-page-s-secret-flying-car-factories>
- [3] K. Nonami, F. Kendoul, S. Suzuki, W. Wang, and D. Nakazawa, Eds., *Autonomous Flying Robots: Unmanned Aerial Vehicles and Micro Aerial Vehicles*. Springer Publisher, 2010.
- [4] Y. B. Sebbane, Ed., *Smart Autonomous Aircraft: Flight Control and Planning for UAV*. CRC Press, 2015.
- [5] T. Ji, S. Chen, R. Varma, and J. Kovacevic, "Energy-efficient route planning for autonomous aerial vehicles based on graph signal recov-

ery,” in *Annual Allerton Conference on Communication, Control, and Computing*, 2015.

- [6] E. Kim, J. Lee, and K. G. Shin, “Real-time prediction of battery power requirements for electric vehicles,” in *IEEE/ACM Intl. Conf. on Cyber-Physical Systems*, 2013.
- [7] A. Cappiello, I. Chabini, E. K. Nam, A. Lue, and M. A. Zed, “A statistical model of vehicle emissions and fuel consumption,” in *IEEE Intelligent Transportation Systems Conf.*, 2002.
- [8] C.-K. Chau, K. Elbassioni, and C.-M. Tseng, “Drive mode optimization and tour planning for plug-in hybrid electric vehicles,” *to appear in IEEE Trans. Intell. Transp. Syst.*, 2017.
- [9] —, “Fuel minimization of plug-in hybrid electric vehicles by optimizing drive mode selection,” in *ACM Intl. Conf. on Future Energy Systems (e-Energy)*, 2016.
- [10] S. Khuller, A. Malekian, , and J. Mestre, “To fill or not to fill: The gas station problem,” *ACM Transactions on Algorithm*, vol. 7, pp. 534–545, 2011.
- [11] N. Christofides, “Worst-case analysis of a new heuristic for the travelling salesman problem,” CMU, Tech. Rep., 1976, report 388, Graduate School of Industrial Administration.
- [12] M. Khonji, M. Alshehhi, C.-M. Tseng, and C.-K. Chau, “Autonomous inductive charging system for battery-operated electric drones,” in *ACM Workshop on Electric Vehicle Systems, Data and Applications (EV-Sys)*, 2017.
- [13] *Helicopter Flying Handbook*. US Federal Aviation Administration, 2012.
- [14] R. K. Ganti, N. Pham, H. Ahmadi, S. Nangia, and T. F. Abdelzaher, “GreenGPS: a participatory sensing fuel-efficient maps application,” in *ACM Mobile Systems, Applications, and Services (Mobisys)*, 2010.
- [15] S. Grubwinkler and M. Lienkamp, “A modular and dynamic approach to predict the energy consumption of electric vehicles,” in *Conf. Future Automotive Technology*, 2013.
- [16] C.-M. Tseng, S. Dsouza, and C.-K. Chau, “A social approach for predicting distance-to-empty in vehicles,” in *ACM Intl. Conf. Future Energy Systems (e-Energy)*, 2014.
- [17] C.-M. Tseng, C.-K. Chau, S. Dsouza, and E. Wilhelm, “A participatory sensing approach for personalized distance-to-empty prediction and green telematics,” in *ACM Intl. Conf. Future Energy Systems (e-Energy)*, 2015.
- [18] C.-M. Tseng and C.-K. Chau, “Personalized prediction of vehicle energy consumption based on participatory sensing,” *to appear in IEEE Trans. Intell. Transp. Syst.*, 2017.

## APPENDIX

**Lemma 1:** In an optimal flight plan  $(\mathcal{T}, b(\cdot))$ , we have<sup>3</sup>

$$\sum_{k=1}^{|\mathcal{T}|-1} \tau(\mathcal{T}_k, \mathcal{T}_{k+1}) + \sum_{k=1: \mathcal{T}_k \in \mathcal{C}}^{|\mathcal{T}|} \tau_c(b(\mathcal{T}_k)) \in [\underline{c}, \bar{c}]d(\mathcal{T}) + c',$$

where either  $\underline{c} = \bar{c} = c_a$  and  $c' = 0$ , or  $\underline{c} = c_a + \underline{c}_f c_b \frac{\eta_d}{\eta_c}$ ,  $\bar{c} = c_a + \bar{c}_f c_b \frac{\eta_d}{\eta_c}$ , and  $c' = \frac{c_b}{\eta_c}(\underline{B} - x_0)$ .  $x_0$  is the initial SoC at  $v_0$ , and  $d(\mathcal{T}) \triangleq \sum_{k=1}^{|\mathcal{T}|-1} d(\mathcal{T}_k, \mathcal{T}_{k+1})$ .

*Proof:* Consider an optimal flight plan  $(\mathcal{T}, b(\cdot))$  and assume that the charging stations, in the order they appear on  $\mathcal{T}$ , is  $\mathcal{T}_{i_1}, \dots, \mathcal{T}_{i_r}$ , where without loss of generality, we assume  $v_0 \neq \mathcal{T}_{i_1}$ . Let  $i_0 \triangleq 1$  and  $i_{r+1} \triangleq |\mathcal{T}|$ . For  $j = 0, 1, \dots, r$ , let

$$D_j \triangleq \eta_d \sum_{k=i_j}^{i_{j+1}-1} c_f(\mathcal{T}_k, \mathcal{T}_{k+1})d(\mathcal{T}_k, \mathcal{T}_{k+1}),$$

and for  $j = 1, \dots, r$ , let  $B_j \triangleq \eta_c b(\mathcal{T}_{i_j})$ .

Then, the feasibility of the tour  $\mathcal{T}$  implies

$$x_0 - \sum_{k=0}^j D_k + \sum_{k=1}^j B_k \geq \underline{B}, \text{ for } j = 0, \dots, r \quad (12)$$

<sup>3</sup>For brevity, we use the notation:  $[\underline{c}, \bar{c}]d(\mathcal{T}) + c'$  to mean the interval  $[\underline{c} \cdot d(\mathcal{T}) + c', \bar{c} \cdot d(\mathcal{T}) + c']$

Let us refer to Ineq. (12) for a particular  $j$  as  $I(j)$ . Consider  $I(r)$ . Suppose that this inequality is not tight, that is, the l.h.s. is strictly larger than the right-hand side. Note that the variable  $b(\mathcal{T}_{i_r}) = \frac{B_r}{\eta_c}$  appears only in this inequality. Since this variable appears in the objective function with a positive coefficient, it has to be set zero at optimality (if the inequality  $I(r)$  is assumed to be strict). If this is the case, then the inequality  $I(r-1)$  becomes redundant; removing this inequality we obtain that the variable  $b(\mathcal{T}_{i_{r-1}})$  appears only in  $I(r)$ . We can conclude that this variable again is zero and remove the (now) redundant inequality  $I(r-2)$  and so on. Continuing this way, we conclude that either all variables  $b(\mathcal{T}_{i_j})$  are set to 0 in which case the value of the objective is  $\tau(\mathcal{T}) = c_a d(\mathcal{T})$ , or we must have

$$x_0 - \sum_{k=0}^r D_k + \sum_{k=1}^r B_k = \underline{B},$$

in which case the value of the objective is

$$\begin{aligned} \tau(\mathcal{T}) + \frac{c_b}{\eta_c} \sum_{k=1}^r B_k &= \tau(\mathcal{T}) + \frac{c_b}{\eta_c} (\underline{B} - x_0 + \sum_{k=0}^r D_k) \\ &= \tau(\mathcal{T}) + \frac{c_b}{\eta_c} \sum_{k=0}^r D_k + \frac{c_b}{\eta_c} (\underline{B} - x_0) \\ &\in \left( c_a + [\underline{c}_f, \bar{c}_f] c_b \frac{\eta_d}{\eta_c} \right) d(\mathcal{T}) + \frac{c_b}{\eta_c} (\underline{B} - x_0). \end{aligned}$$

**Theorem 2:** The flight plan  $(\mathcal{T}, b'(\cdot))$  returned by Algorithm Find-plan $[V, d]$  has cost

$$\tau(\mathcal{T}) + \tau_c(b(\mathcal{T})) = O(\text{OPT}_{\text{DFP}}) + O(1).$$

*Proof:* Let  $(\mathcal{T}^*, b^*(\cdot))$  be an optimal flight plan for (DFP). Clearly, this plan can be trivially turned into a feasible solution  $(\mathcal{T}^*, x)$  for (SDFP) by setting  $x_k = \bar{B}$  for all  $\mathcal{T}_k \in \mathcal{C}$ . It follows that

$$\text{OPT}_{\text{SDFP}} \leq d'(\mathcal{T}^*). \quad (13)$$

On the other hand, Lemma 2 implies that

$$d'(\mathcal{T}) \leq \frac{3}{2} \left( \frac{1+\alpha}{1-\alpha} \right) \text{OPT}_{\text{SDFP}}. \quad (14)$$

Lemma 1 also implies that

$$\text{OPT}_{\text{DFP}} \geq \underline{c} \cdot d(\mathcal{T}^*) + c', \quad (15)$$

while Corollary 1 implies that

$$b(\mathcal{T}) \leq \frac{B - x_0}{\eta_c} + \frac{\bar{c}_f \eta_d}{\eta_c} d(\mathcal{T}), \quad (16)$$

and the definition of  $d'(\cdot, \cdot)$  implies

$$\underline{c}_f d(\mathcal{T}) \leq d'(\mathcal{T}) \text{ and } d'(\mathcal{T}^*) \leq \bar{c}_f d(\mathcal{T}^*). \quad (17)$$

Putting together (13), (14), (15), (16), and (17), we obtain

$$\begin{aligned} \tau(\mathcal{T}) + \tau_c(b(\mathcal{T})) &= c_a d(\mathcal{T}) + c_b b(\mathcal{T}) \\ &\leq \left( c_a + \bar{c}_f c_b \frac{\eta_d}{\eta_c} \right) d(\mathcal{T}) + c_b \frac{B - x_0}{\eta_c} \\ &\leq \frac{3}{2} \left( \frac{1+\alpha}{1-\alpha} \right) \frac{\bar{c}_f}{\underline{c}_f} \left( c_a + \bar{c}_f c_b \frac{\eta_d}{\eta_c} \right) \left( \frac{\text{OPT}_{\text{DFP}} - c'}{\underline{c}} \right) + c_b \frac{B - x_0}{\eta_c} \end{aligned}$$